Journal of Hydro-environment Research xxx (xxxx) xxx–xxx

Contents lists available at ScienceDirect

Journal of Hydro-environment Research

journal homepage: www.elsevier.com/locate/jher

Nappe flows on a stepped chute with prototype-scale steps height: Observations of flow patterns, air-water flow properties, energy dissipation and dissolved oxygen

Stefan Felder[a,*], Margaux Geuzaine[b], Benjamin Dewals[c], Sebastien Erpicum[c]

[a] Water Research Laboratory, School of Civil and Environmental Engineering, UNSW Sydney, 110 King St, Manly Vale, NSW 2093, Australia
[b] Structural and Stochastic Dynamics (SSD), ArGEnCo Department, Liege University, Allée de la Découverte, 13 – B52, B-4000 Liege, Belgium
[c] Hydraulics in Environmental and Civil Engineering (HECE), ArGEnCo Department, Liege University, Allée de la Découverte, 13 – B52, B-4000 Liege, Belgium

ARTICLE INFO

Keywords:
Air-water flows
Dissolved oxygen
Nappe flows
Physical modelling
Prototype-scale steps height
Stepped spillway

ABSTRACT

Air-water flows occur commonly in stepped spillways including the nappe flow regime for low flow rates. The present laboratory experiments researched the nappe flow regime in a stepped chute with prototype-scale steps height providing unique insights into the evolution of nappe flows along a stepped chute. Detailed visual observations highlighted the varying flow features along the stepped chute including the evolution of flow aeration, of jet properties and of instationarities in form of jump waves and cavity fluctuations with typical frequencies of around 1 Hz. These instationarities were caused by complex flow interactions at the impingement of the jet on the horizontal step face. Detailed air-water flow measurements revealed the complexity of the flows highlighting both S-shape and jet-like void fraction distributions and jet-like interfacial velocity distributions downstream of the jet impact and at step edges. This resulted in a downwards shift of the bubble count rate distributions closer to the step face. The nappe flows showed strong energy dissipation and reaeration performances along the stepped chute. The present study provided a robust and extensive characterisation of nappe flows and due to the large scale of the experiments, the results should provide confidence for the design of stepped chutes with embankment dam slope.

1. Introduction

Stepped cascades have been the subject of extensive study over decades (e.g. Chanson, 1995; Chanson et al., 2015). Flows on stepped chutes are characterized by strong energy dissipation and complex interactions between air and water entities within the flows downstream of the inception point of free-surface aeration (e.g. Gonzalez and Chanson, 2008; Bung and Valero, 2016; Felder and Chanson, 2016a; Zhang and Chanson, 2018). Stepped spillways for flood mitigation purposes are typically designed for maximum flow conditions, which take place in the skimming flow regime. Research has particularly focused on such skimming flows which are characterized by stable recirculation motions within the step cavities (e.g. Rajaratnam, 1990; Meireles and Matos, 2009; Felder and Chanson, 2011; Bayon et al., 2018).

For intermediate flow rates, the flow may be characterized by instationary and unstable motions in the transition flow regime which is associated with unsteady movements of air pockets within the step cavities and associated cavity ejection processes (Ohtsu and Yasuda, 1997; Chanson and Toombes, 2004; Felder and Chanson, 2015a; Kramer and Chanson, 2018). For the lowest flow rates, in the nappe flow regime, the flows propagate along the stepped chute as a succession of free-falling jets or nappes (Horner, 1969; Chamani and Rajaratnam, 1994; Chanson, 1995) (Fig. 1). Spillways with mild slopes may be designed to operate in the nappe flow regime to reaerate oxygen-depleted waters (Essery et al., 1978; Toombes and Chanson, 2005; Baylar et al., 2007) (Fig. 1b). While steep stepped spillways are typically not designed for nappe flows, in the lead up to higher design flow rates any stepped chute is exposed to a nappe flow regime at least temporarily.

Researchers have differentiated between two nappe flow sub regimes comprising nappe flows with hydraulic jumps and without hydraulic jumps (Chanson et al., 2015). For the first case, the energy dissipation along the stepped chute may be expressed as a succession of single steps (Moore, 1941; Rand, 1955; Chanson, 1995) combining the individual energy dissipation contributions of a free-falling jet and a

* Corresponding author.
E-mail addresses: s.felder@unsw.edu.au (S. Felder), mgeuzaine@uliege.be (M. Geuzaine), b.dewals@uliege.be (B. Dewals), s.erpicum@uliege.be (S. Erpicum).

https://doi.org/10.1016/j.jher.2019.07.004
Received 27 November 2018; Received in revised form 13 April 2019; Accepted 22 July 2019

Notation

a	Interfacial area (1/m)
b	coefficient of maximum variation in chord sizes
C	Void fraction
C_d	Dissolved oxygen concentration in step cavity (mg/L)
C_{mean}	Cross-sectional mean void fraction: $C_{mean} = \frac{1}{Y_{90}} \times \int_0^{Y_{90}} C \times dy$
C_{Fmax}	Void fraction corresponding to location of maximum bubble count rate
C_s	Dissolved oxygen concentration at saturation (mg/L)
C_u	Dissolved oxygen concentration at the upstream end (mg/L)
ch_{air}	Average chord sizes of air bubbles (m)
ch_{water}	Average chord sizes of water droplets (m)
d	Equivalent clear water flow depth (m): $d = \int_0^{Y_{90}} (1 - C) \times dy$
d_c	Critical flow depth (m)
d_{pool}	Water depth in step cavity (m)
d_{pool}'	Fluctuations of water depth in step cavity (m)
E_{20}	Aeration efficiency at 20 °C
F	Bubble count rate (Hz)
F_{max}	Maximum bubble count rate in a cross-section (Hz)
g	Gravity acceleration constant (m^2/s)
H	Total head (m)
H_{dam}	Height of dam to respective step (m)
H_{max}	Maximum upstream head (m) above chute toe
H_{res}	Residual energy (m)
h	Step height (m)
L	Step length (m)
L_{Jet}	Distance from the start of a step cavity to the midpoint of the impinging jet (m)
$L_{Jet,\min}$	Distance from the start of a step cavity to the minimum of the impinging jet (m)
N	Number of steps
Q	Flow rate (m^3/s)
q_w	Specific flow rate (m^2/s)
Re	Reynolds number defined in terms of the hydraulic diameter (-)
U_w	Equivalent clear water flow velocity (m/s): $U_w = \frac{q_w}{d}$
V	Interfacial velocity (m/s)
V_{90}	Characteristic interfacial velocity where $C = 0.9$ (m/s)
W	Channel width (m)
y	Coordinate perpendicular to horizontal step face (m)
y_{Fmax}	Flow depth corresponding to location of maximum bubble count rate (m)
Y_{90}	Characteristic flow depth where $C = 0.9$ (m)
θ	Slope of spillway
ν	Kinematic viscosity (m^2/s)

hydraulic jump (Peyras et al., 1992; Chanson, 1994). Experimental evidence suggests however that this sub regime only occurs for very low flow rates while the more common nappe flow regime is without hydraulic jumps and supercritical flow throughout. Little research on the development and propagation of the flow properties along stepped cascades under such flow conditions exists albeit research by Chanson and Toombes (2002a) on a stepped chute with ventilated first step cavity and slope $\theta = 3.4°$. As emphasized by Chanson et al. (2015), the ventilation of the first step cavity may prevent instabilities along the stepped chute which may be caused by nappe oscillations. In contrast to this statement, Essery and Horner (1978) reported that there is no effect of cavity ventilation for nappe flows without hydraulic jump. Many prototype stepped spillways with mild slope and without ventilated first step cavity have performed well (Fig. 1). While nappe flows for very low flow rates appear regular, with increasing flows some instabilities may be observed within the nappe flow regime at both laboratory and prototype scale. Herein the present study provides detailed observations of nappe flows without hydraulic jumps along a stepped chute without ventilation of the first step cavity, providing a unique data set for the evolution of such flows along a stepped chute including the propagation of instabilities and the establishment of equilibrium air-water flow parameters.

Despite its relevance for any stepped chute, research of the nappe flow regime is limited. Table 1 summarizes past experimental studies of nappe flows including information about the chute slope θ, the step height h, the channel width W and the discharge per unit width q_w. Table 1 lists also the focus of previous experimental studies including the observations of the flow patterns (e.g. Peyras et al., 1992; Toombes and Chanson, 2008a), the threshold levels of occurrence of the nappe flow regime (e.g. Pinheiro and Fael, 2000; Renna and Fratino, 2010; Chanson et al., 2015) and the energy dissipation performance (e.g. Stephenson, 1991; Chamani and Rajaratnam, 1994; Chanson, 1994; Pinheiro and Fael, 2000). Research of flow patterns suggests that nappe flows with hydraulic jumps may be very similar from step to step (Fig. 1), while research by Toombes and Chanson (2008a) highlighted the three-dimensional nature of nappe flows without hydraulic jump ($\theta = 3.4°$) including sidewall standing waves and shockwaves which do not reach equilibrium flow conditions. Herein the present study adds missing research of flow patterns on a steeper sloped stepped spillway ($\theta = 15°$) in nappe flows without hydraulic jumps.

Also, very little research has been conducted of the air-water flow properties in nappe flows despite research by Toombes and Chanson (2005, 2008b) and the recording of some basic air-water flow properties by Takahashi et al. (2007) on a stepped spillway with $\theta = 19°$. Herein the present study investigated the air-water flow properties and energy dissipation performances in nappe flows systematically along a stepped chute with prototype-scale steps height.

Several studies have also measured the re-aeration efficiency of stepped cascades including direct dissolved oxygen measurements (Essery et al., 1978; Toombes and Chanson, 2005; Baylar et al., 2007) and indirect quantification via air-water flow data (Toombes and Chanson, 2005; Felder and Chanson, 2015b). Direct measurements of aeration efficiency along a stepped cascade were conducted with instrumentation at the upstream and downstream ends of the stepped chute ignoring the flow processes and the evolution of reaeration in between. Herein, the present study provided a more detailed picture of the reaeration along a stepped cascade measuring the aeration efficiency with several dissolved oxygen meters distributed along the stepped chute. The present study investigated the interaction between air-water flow properties, dissolved oxygen concentration and energy dissipation providing the most detailed characterization of nappe flows to date. To limit potential scale effects in the air-water flows which have been reported on stepped spillways (Kobus, 1984, Felder and Chanson, 2017), the stepped chute in the present study consisted of a series of steps with prototype-scale height.

2. Experimental facility and instrumentation

New nappe flow experiments were conducted at HECE Laboratory, University of Liege in a stepped spillway model with 6 identical prototype-scale steps with height $h = 0.5$ m, length $L = 1.87$ (i.e. $\theta = 15°$) and width $W = 0.2$ m (Fig. 2a). The model represented a slice of a 157 m wide aerating weir built downstream of a large dam in Cameroon to increase the dissolved oxygen concentration (Erpicum et al., 2016) (Fig. 1b). The horizontal step faces as well as the broad-crested weir upstream of the first step edge were made of rubble masonry, consistent

(a) Stepped spillway of Gold Creek Dam (Brisbane, Australia) operating in nappe flows with hydraulic jump in April 2015 (step height $h = 1.5$ m, spillway slope $\theta = 21°$)

(b) Stepped spillway of the Lom River (Cameroon), downstream of the Lom Pangar Dam operating in nappe flows without hydraulic jump in November 2016 ($h = 0.5$ m, $\theta = 15°$, flow rate $Q \approx 100$ m^3/s) (Photo courtesy of Thibaut Guillemot, ISL Ingénierie)

Fig. 1. Nappe flow regime in prototype stepped spillways.

with the prototype weir. The vertical step faces and one of the sidewalls were made of PVC, while the other sidewall was made of Perspex for flow visualisation.

The water supply system of the laboratory was a closed loop with regulated pumps and an underground reservoir with a 400 m^3 maximum volume. The reservoir was filled with tap water. Water was pumped from the underground reservoir to the 1 m long, 1 m wide and 3 m high upstream header tank via a submerged supply pipe. A smooth contraction channelled the flows calmly into the experimental test section via a broad-crested weir of length 1.01 m (Fig. 2a). Downstream of the model, an open channel returned the water to the underground reservoir. The discharge was measured using an electromagnetic SIEMENS MAG 5100 flow meter on the 0.15 m diameter supply pipe (accuracy of 0.5% at full scale).

Extensive measurements of the air-water flow properties along the stepped chute were conducted with a double-tip conductivity probe which was designed at the Water Research Laboratory, UNSW Sydney and recently benchmarked against commonly used RBI fiber-optical probes (Felder and Pfister, 2017; Felder et al. 2019). The conductivity probe had two identical needle tips with inner electrodes of 0.125 mm diameter which were separated in streamwise and transverse directions by 5.8 mm and 1 mm respectively. The raw data were acquired with a NI-9222 data acquisition system and LabVIEW software sampling both sensors simultaneously for 45 s and at 20 kHz, as recommended by Felder and Chanson (2015a). The raw voltage data were post-processed with the Fortran software of Felder (2018) providing the full range of air-water flow properties including void fraction C, bubble count rate F, interfacial velocity V and interfacial area a. The calculation of C and F was based upon a single threshold technique using a 50% threshold of the bimodal peaks of the raw voltage signals of the conductivity probe. Herein C represented the average void fraction which is the time a probe tip spends in the air phase over the sampling duration, while the bubble count rate provided the average number of changes from the air to the water phase (and from the water to the air phase) per second. The

Table 1
Previous experimental studies of nappe flows on stepped spillways; summary of flow conditions and main research focus.

Reference	θ [°]	h [cm]	W [m]	q_w [m^2/s]	Flow patterns	Flow regime change	Energy dissipation	Air-water flow properties	Re-aeration	Comment
Horner (1969); Essery and Horner (1978)	11.3–45	2.9–50	0.15, 0.3, 0.6		✓	✓	✓			Flat and inclined steps
Essery et al. (1978)	11.3, 21.8, 45	5, 10, 25, 50	0.15	0.012–0.145					✓	Flat and inclined steps
Stephenson (1979)	18.4, 26.6, 45	10, 15	0.1, 0.38				✓			Gabbion stepped spillway
Sorensen (1985)	52	2.4, 6.1	0.3	0.005–0.235	✓		✓			Physical modell of Monksville Dam
Stephenson (1991)	54.5						✓			Kennedy's vale model
Peyras et al. (1992)	18.4, 26.6, 45	100	0.8	0.06–0.25	✓		✓			Gabbion stepped spillway with various modifications
Pinheiro and Fael (2000)	14, 18.4	5	0.7	0.004–0.057		✓	✓			
Chanson and Toombes (2002a)	3.4	7.1, 14.3	0.5	0.04–0.15	✓		✓	✓		Upward inclined steps
Chinnarasri and Wongwises (2004)	30, 45, 60	7.5, 10.6, 13	0.4	0.01–0.17	✓	✓	✓			
Toombes and Chanson (2005)	2.6, 3.4	7.1, 14.3	0.25, 0.5	0.04–0.15				✓	✓	Multistep and single step data
Takahashi et al. (2007)	19	0.625–5	0.4	0.0001–0.099			✓	✓		Dimensions as per Ohtsu et al. (2004)
Baylar et al. (2007)	14.5–50	5–15	0.3	0.017–0.17		✓			✓	
Toombes and Chanson (2008a, b)	2.6, 3.4	7.1, 14.3	0.25, 0.5	0.04–0.15	✓			✓		Multistep and single step data
Renna and Fratino (2010)	14–45	20	0.6	0.008–0.42	✓	✓	✓			
Present study	15	50	0.2	0.005–0.637	✓		✓	✓	✓	Horizontal step face of rubble masonry

interfacial velocities were calculated based upon a cross-correlation analysis of the simultaneously sampled leading and trailing tips of the conductivity probe which provided the average travel time of air-water interfaces between the two probe tips. The interfacial area, i.e. the area between the air and water phases, was calculated based upon the air-water flow data as $a = 4 \times F/V$. Both bubble count rate and interfacial area are important for the estimation of the reaeration efficiency of air-water flows. Further details on the data processing and the air-water flow properties can be found in Chanson and Toombes (2002b) and Felder (2013). Air-water flow measurements were conducted along the stepped chute in the channel centerline, including at all step edges as well as two positions towards the downstream end of the step cavity, i.e. locations where the flow was parallel to the horizontal step face (Table 2, Fig. 2b). These two locations comprised two equally spaced positions downstream of the center point of the impinging jet at each step edge L_{Jet}, i.e. step edge – $2/3 \times (L - L_{Jet})$ and step edge – $1/3 \times (L - L_{Jet})$ (Fig. 2b). The measurement accuracy of the conductivity probe provided void fractions within $\Delta C/C = 4\%$ and interfacial velocities within $\Delta V/V = 10\%$. The accuracy was assessed in comparative analyses with other commonly used phase-detection probes (Felder and Chanson, 2016b; Felder and Pfister, 2017; Felder et al. 2019). Further research for the operation of all types of phase-detection intrusive probes in high-velocity air-water flows is needed to determine their accuracy more comprehensively.

Direct measurements of the dissolved oxygen concentrations along the stepped chute were conducted with 6 identical HACH LDO sensors (optical measure by luminescence with an accuracy of ± 0.2 mg/l according to the probe manufacturer). The sensors sampled with a frequency of 1 Hz and the signal was acquired with portable HACH multi meters HQ40D. The sensors were located within the step niches along the stepped chute, just upstream of the minimum jet impact with length $L_{Jet,min}$ (Fig. 2b), including at the upstream and downstream ends of the chute and in several step cavities. Additional tests were conducted at several positions along the same step cavity to document the evolution of dissolved oxygen concentration along a single cavity. Additional oxygen concentration measurements were conducted by Winkler tests performed on water samples from different locations along the spillway. A comparison of these tests with the dissolved oxygen probes confirmed the accuracy and proved limited influence of air bubbles on the sensors (differences less than 0.2 mg/l). Erpicum et al. (2016) summarized the dissolved oxygen measurements in more detail and presented preliminary results. Table 2 summarizes the experimental flow conditions for the direct measurements of dissolved oxygen.

Detailed observations of the flow patterns were documented with a video camera (Canon Legria HF R68) and a digital camera (Panasonic DMC-GH4) for a wide range of unit discharges $0.005 < q_w < 0.637$ m^2/s corresponding to Reynolds numbers Re defined in terms of the hydraulic diameter $2 \times 10^4 < \text{Re} < 2.5 \times 10^6$. The visual observations of the flow patterns revealed fluctuations of the water level within the step cavities and time series of the pressure variations within the step cavity were recorded with a pressure sensor (Keller PR-41X 0–0.1 bar, accuracy of $\pm 10^{-4}$ bar according to the sensor manufacturer). The pressure sensor was installed behind the vertical step face at an elevation of about 2–3 cm above the horizontal step face. The sensor was connected to a NI USB 9210 data acquisition unit and the raw pressure data within the step cavity were acquired with LabVIEW Signalexpress for at least 30 min at 100 Hz. The post-processing of the cavity pressure signals yielded the mean flow depth in the cavity d_{pool}, the standard deviation of the flow depth d_{pool}' and the characteristic frequencies of the fluctuations in each cavity.

Table 2 provides an overview of the flow conditions and the conducted measurements in the present study including the dimensionless discharge d_c/h, where d_c is the critical flow depth. Note that the flows at step edge 1 were unaerated. The two-dimensionality of the flows across the width of the chute were verified with additional profiles of air-

(a) Overview of stepped spillway model (dimensions in m) with numbering of step edges and step cavities (italic numbers)

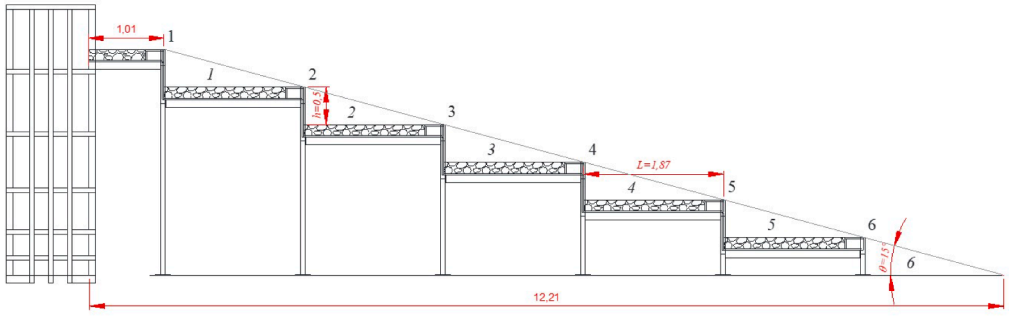

(b) Definition of step cavity parameters and measurement locations

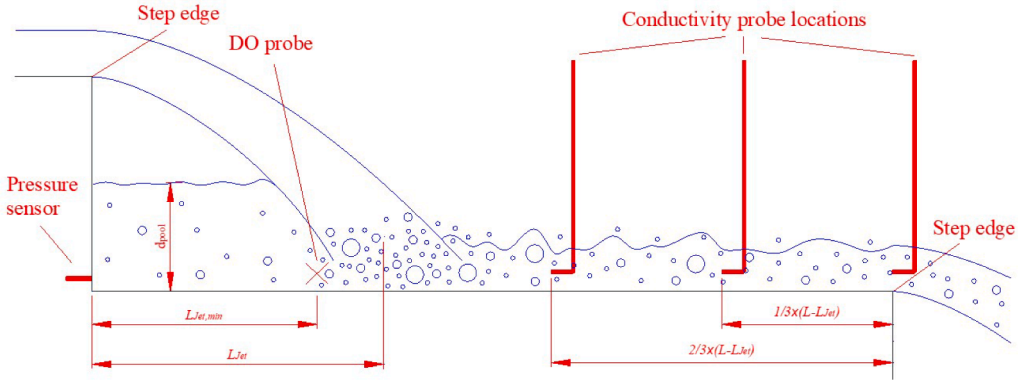

Fig. 2. Sketches of the experimental setup in the present study.

Table 2
Summary of nappe flow conditions and experimental measurements in the present study (all experiments in channel centerline) (CP = conductivity probe; PS = pressure sensor; DO = dissolved oxygen sensor).

d_c/h (–)	Air-water flow properties along chute (CP)	Energy dissipation at last step edge (CP)	Cavity processes along chute (PS)	Dissolved oxygen in cavities along chute (DO)
0.162	✓	✓	✓	
0.274	✓	✓	✓	✓
0.360		✓		
0.436	✓	✓	✓	✓
0.506		✓		
0.571	✓	✓	✓	✓
0.632		✓		
0.668				✓
0.692	✓	✓	✓	✓

water flow properties at locations $1/4 \times W$ and $3/4 \times W$ for all discharges and towards the downstream end of the flume. For the smallest flow rates, some small flow bulking towards the sidewalls of the flume was observed which decreased for the largest nappe flow rates.

3. Flow patterns

For a range of unit discharges $0.005 < q_w < 0.637\,m^2/s$ ($0.027 < d_c/h < 0.692$) detailed observations of the flow patterns were conducted including visual observations of the propagation of jets along the stepped chute, of the pool depths and fluctuation frequencies in the step cavities and of the lengths of the jets. The observations provided the most detailed report of nappe flow patterns along a stepped chute to date. To highlight the air-water flow patterns in the nappe flow regime, four movies are provided as supplementary material presenting the flow features for discharges of $d_c/h = 0.13$, $q_w = 0.05\,m^2/s$ (Movie 1), $d_c/h = 0.27$, $q_w = 0.16\,m^2/s$ (Movie 2), $d_c/h = 0.44$, $q_w = 0.32\,m^2/s$ (Movie 3) and $d_c/h = 0.69$, $q_w = 0.64\,m^2/s$ (Movie 4).

3.1. Visual observations of flow patterns

3.1.1. Nappe flows with hydraulic jump

For all flow conditions, a nappe flow regime was observed. For the smallest flow rates $q_w \leq 0.015\,m^2/s$ ($d_c/h \leq 0.057$), the flow patterns resembled a nappe flow regime with hydraulic jumps. The flows were very regular with a distinct pattern of clear water flows upstream of each step edge followed by a 2-dimensional jet which impacted upon the horizontal step face underneath. The jet impact led to small flow aeration, to the filling of the cavity underneath the nappe with a small layer of water which varied slightly in depth and on the other side to the formation of a hydraulic jump with undulations and standing waves which transitioned the flows to subcritical before the next step edge. The jet was stable and there was no aeration along the jet, while small amounts of air were entrained at the impingement point. The nappe flows appeared very regular along the flume and agreed well with the commonly applied definition of a nappe flow regime with hydraulic jump (NA1) highlighting that for such low flow rates, an analysis of the

energy dissipation may be regarded as a succession of free-falling jets (Chanson, 1995).

3.1.2. Nappe flows without hydraulic jump

For larger flow rates, i.e. $0.015 < q_w \leq 0.637\ m^2/s$ ($0.057 < d_c/h \leq 0.692$), nappe flows without hydraulic jump were observed and the flows remained supercritical throughout. Note that $q_w = 0.637\ m^2/s$ was the maximum possible flow rate in the present study and no onset of transition flows was observed. The observation of the nappe flow regime for these flow conditions was consistent with data from the literature for the presence of nappe flows (References in Table 1; Chanson et al., 2015; Kramer and Chanson, 2018).

The present observations confirmed that nappe flows without hydraulic jump should not be simply regarded as the succession of equal free-falling jets. While the flows looked steady and equal from top view, i.e. the flows appeared to exist of a succession of equal fully aerated jets along the stepped chute, the observations through the side wall highlighted the evolution of the nappe flows along the stepped chute (Fig. 3; Movies 1–4). Visual observations showed that the lengths of the jets, the flow aeration and instabilities increased along the stepped chute. Towards the downstream end of the stepped chute (i.e. downstream of step edge 4), visually, the flow aeration, the jet lengths and the cavity properties appeared to reach some equilibrium while some instable jump waves and the ejection of droplets above the flume continued to increase. With increasing discharge, the flows became more instable including unstable cavity processes, intermittent closing of step cavities at the upstream end of the chute as well as instationary propagation of small jump waves along the chute associated with strong splashing (Figs. 4 and 5; Movies 3 and 4). The nappe flows in the present study resembled features typically referred to in transitions flows. This observation is significant since it highlights that the nappe flow regime without hydraulic jump can be partially unsteady and careful design considerations need to be applied. The present observations appear to be consistent with the flow patterns description in Essery and Horner (1978). Observations on prototype stepped chutes in nappe flows also confirm the present observations of irregular and varying nappe flow patterns (Fig. 1b and Fig. 8 in Chanson and Toombes, 1998).

For all nappe flows without hydraulic jump, the flow remained unaerated upstream of step edge 1 and further downstream the flows were aerated throughout. Air was entrained at the impingement point of the jet upon the horizontal step face (Fig. 3; Movies 1–4), along the jet itself (e.g. Fig. 4; Movies 1–4) and along the free-surface of the supercritical flows on the horizontal step face (Movies 1–4). With increasing flow rate, the flow aeration increased. Downstream of the impingement point a large standing wave existed for the lower flow rates ($d_c/h < 0.2$) (Fig. 3a; Movie 1), while strong aeration and equal flow bulking was observed for larger flow rates (Fig. 3b; Movies 3 and 4). The impingement of the jet resulted in highly unstable entrainment and recirculation motions (Figs. 3 and 4; Movies 1–4) which resulted in irregular air entrainment into the step cavity and strong flow aeration of the flows in the downstream part of the step face. With increasing discharge, the jet length and the width of the jet increased (Fig. 3; Movies 1–4). Within each step cavity, some unaerated waters pooled in front of the vertical step face; the water levels increased with increasing flow rate and decreased along the stepped chute (Fig. 3; Movies 1–4). The waters within the step cavity fluctuated linked with the irregular impingement of the jet upon the horizontal step face. The combination of irregular impingement and cavity fluctuations resulted in instationarities including jump wave propagation along the stepped chute and strong droplet ejections of about 4 times step height (Fig. 4; Movies 1–4). With increasing flow rate and with increasing distance along the stepped chute, the jump wave instabilities and the splashing increased, while the intensities of the water level fluctuations within the cavities did not increase. The present observations indicated that the nappe flow instabilities were not caused by the unventilated step cavities, but by complex interactions between jet impingement, step cavity fluctuations and amplifications along the stepped chute, rather than by jet oscillations due to an unventilated first step cavity.

(a) Jet impact downstream of step edge 4 with clear water in the step cavity and strong aeration and flow bulking downstream of the jet impact: $q_w = 0.073\ m^2/s$, $d_c/h = 0.162$, $Re = 2.9 \times 10^5$

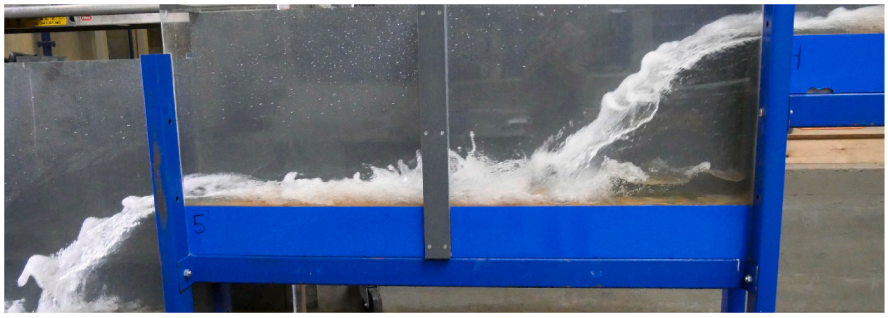

(b) Increasing aeration and instabilities along stepped chute: $q_w = 0.319\ m^2/s$, $d_c/h = 0.436$, $Re = 1.3 \times 10^6$

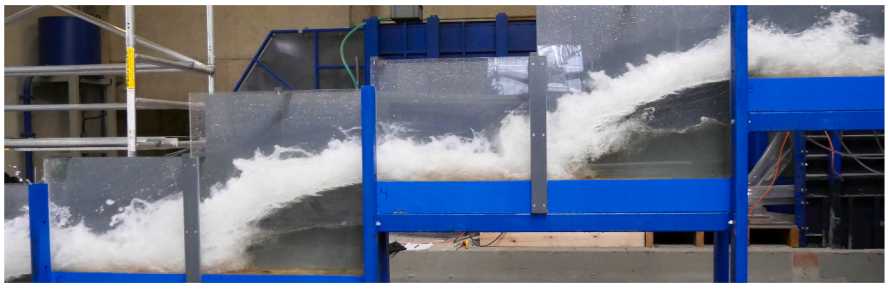

Fig. 3. Photos of evolution of nappe flows in present study.

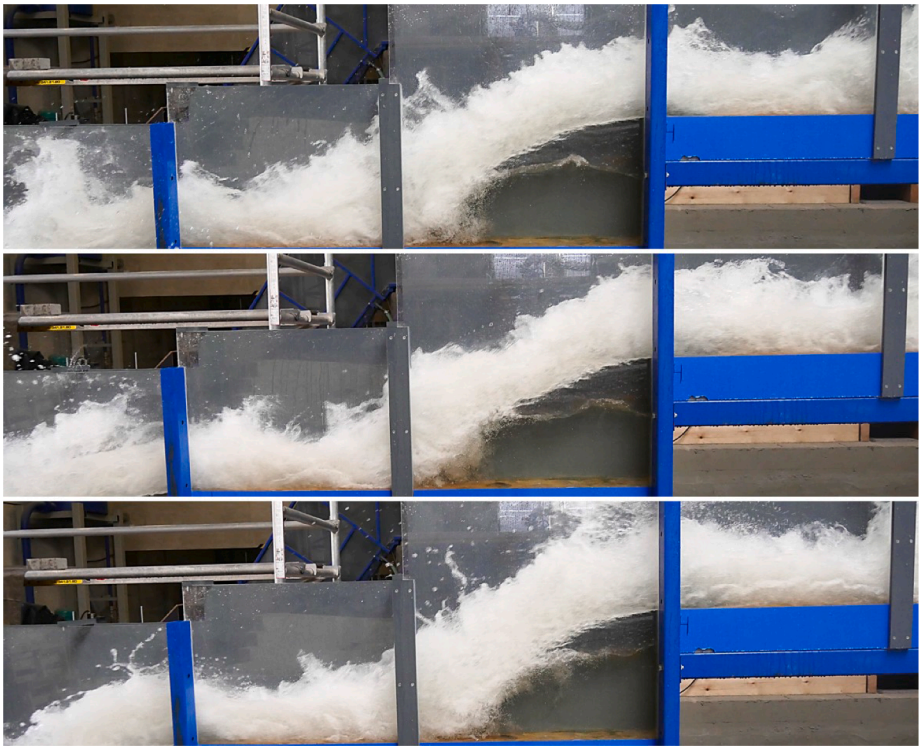

Fig. 4. Photo sequence of instabilities and droplet ejections along the stepped chute: $q_w = 0.637\ m^2/s$, $d_c/h = 0.692$, Re = 2.6×10^6 (irregular time step between images of a few seconds).

For $d_c/h = 0.38$, the cavity downstream of the first step edge was fully filled with water intermittently resulting in a change in flows within the step cavity, i.e. stable recirculation motions as typical for skimming flows. The filling of the cavity with water was not regular and appeared random. For $d_c/h > 0.43$, the step cavity downstream of step edge 1 was permanently filled with water, while the other step cavities remained unaerated. For $d_c/h = 0.608$, the step cavity downstream of step edge 2 became intermittently and randomly filled with waters (Fig. 5). When the step cavity was aerated, small amounts of air were entrained into the step cavity, while a fully submerged cavity resulted in intense aeration and unsteady recirculation motions within the step cavity (Fig. 5). A similar process was observed for $d_c/h = 0.69$, where the step cavity downstream of step edge 3 became intermittently and randomly filled with waters (Movie 4). These unsteady processes contributed to the instationary jump waves along the chute.

3.2. Lengths of the jets

Downstream of each step edge, the jet impacted upon the underlying horizontal step face. With increasing flow rate, the jets increased in size linked with increasing flow aeration (Figs. 3 and 4). The jet lengths L_{Jet} was defined as the distance from the step edge to the center of the impinging jet (Fig. 2b). The jet lengths were observed visually for a range of flow conditions with an accuracy of ± 2 cm independent of the flow conditions. Fig. 6 summarizes the dimensionless jet lengths L_{Jet}/h as a function of d_c/h. The data highlighted an increase in jet lengths with increasing discharge as well as an increase in L_{Jet} along the flume. Towards the downstream end of the flume, i.e. downstream of step edge 4, the jet lengths were close indicating that the flows approached uniform flow conditions (Fig. 6). With increasing discharge, step cavities at the upstream end became intermittently and then fully

Fig. 5. Photo sequence of instable cavity processes in cavity downstream of step edge 2: $q_w = 0.525\ m^2/s$, $d_c/h = 0.608$, Re = 2.1×10^6 (irregular time step between images of a few seconds).

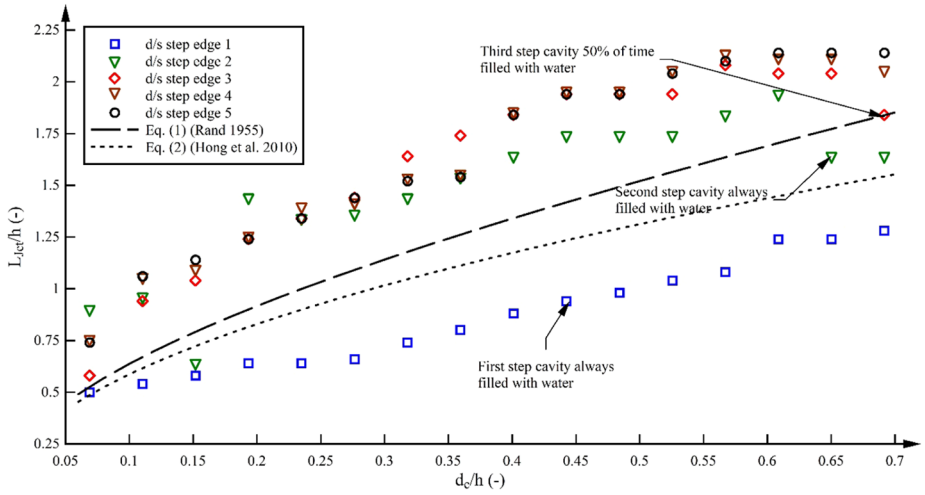

Fig. 6. Development of jet lengths along the stepped chute downstream (d/s) of step edges; Comparison with equations for ventilated nappes (Eqs. (1) and (2)).

filled with waters which resulted in a reduction of jet lengths at subsequent step edges (Fig. 6).

The present data were compared with the well-accepted equation of Rand (1955) who expressed the jet length above a ventilated cavity as:

$$\frac{L_{Jet}}{h} = 1.98 \times \sqrt{\frac{d_c}{h} \times \left(1 + 0.357 \times \frac{d_c}{h}\right)} \quad (1)$$

The data were further compared with the semi-empirical equation by Hong et al. (2010) for ventilated jets:

$$\frac{L_{Jet}}{h} = 1.855 \times \sqrt{\frac{d_c}{h}} \quad (2)$$

While the present data followed a similar trend compared to Eqs. (1) and (2), some clear differences were observed (Fig. 6). The authors believe that these differences were caused by the unventilated first step cavity. The data at subsequent step edges were not directly comparable since Eqs. (1) and (2) were only developed for the first ventilated jet. Downstream of the first drop, all present jet conditions were fully aerated and hence not directly comparable.

3.3. Depths and frequencies in step cavities

Visual observations included also the average flow depth in the cavities, which were assessed with an accuracy of ± 5 mm. Fig. 7a illustrates all observations of the dimensionless water depth d_{pool}/h as a function of d_c/h for a wide range of nappe flow discharges without hydraulic jump (hollow symbols). The observations highlighted an increase in flow depth with increasing discharge and a decrease in flow depth along the stepped chute. For $d_c/h = 0.43$, the first step cavity was always filled with water resulting in a constant water depth for higher discharges, while the same occurred for the second step cavity at higher discharges (Fig. 7a). The present data were compared with an analytical solution by Rand (1955) for a fully ventilated jet. While the data were in good agreement for the lowest discharges ($d_c/h < 0.3$), with the intermittent filling of the step cavity with water, the differences increased. The present observations highlighted that the theoretical solution of the jet properties for a ventilated jet cannot be directly applied to an unventilated jet cavity and that care must be taken. Also, the theory was not applicable at any subsequent step cavity since the water became fully aerated downstream of the first step edge.

The water elevation d_{pool}/h in the step cavities were also directly estimated with a pressure sensor installed within the vertical step face and the data are also shown in Fig. 7a (bold symbols). Both visual observations and pressure data were in good agreement for the lowest flow rates, while some differences were observed for the larger flow rates ($d_c/h > 0.4$). These differences were linked with the strong fluctuations of the water levels within the step cavity and the difficulty to record these fluctuations visually as well as some fundamental flow processes. For the larger flow rates, the pressure data were below the visual water levels (Fig. 7a). For these flow conditions, the step cavities were intermittently or always filled with water resulting in stable recirculation movements within the cavity similar to typical skimming flow observations (Felder and Chanson, 2011). As reported by Sanchez-Juny et al. (2000), in a skimming flow regime, the pressures within the step cavity may be reduced due to such recirculation motions. For the lowest nappe flows in the present study, the pressure was hydrostatic within the step cavity, i.e. the pressure measured by the pressure sensor was equal to the elevation of the water level d_{pool}. For a fully filled step cavity, the pressure was no more hydrostatic because of the recirculation in the cavity and the jet effects and the measured pressure was smaller than d_{pool} (Fig. 7a).

Fig. 7b illustrates the fluctuations of the flow depth d_{pool}'/h in the step cavities recorded with the pressure sensor where d_{pool}' is the standard deviation of the water depth in the step cavity. Fig. 7b highlights an increase in fluctuations of the water depth in the step cavities with increasing discharge. While some variations in values were observed, the fluctuations remained overall stable along the stepped chute.

For all raw data, FFT analyses identified the characteristic frequencies of the cavity movements. Fig. 7c illustrates all characteristic frequencies in the step cavities along the stepped chute including the dominant frequencies (bold symbols) as well as secondary frequencies (hollow symbols). Note that for some flow conditions several frequencies were identified including two dominant frequencies. For the first step cavity, no characteristic frequencies were identified. For all nappe flow rates in the present study, a dominant frequency between 0.75 and 1.3 Hz was observed; the characteristic frequencies decreased slightly along the stepped chute (Fig. 7c). For the smallest flow rates, an additional dominant frequency of about 4–4.5 Hz was observed, while several secondary frequencies were found between 1.5 and 4 Hz (Fig. 7c).

The frequency analysis yielded well-defined frequency spikes of the water depth fluctuations within the step cavities. It is believed that these cavity frequencies resembled the characteristic frequencies of the jump waves. Visual observations confirmed the occurrence of jump waves approximately every second, which is consistent with the observation of the dominant frequency of about 0.75–1.3 Hz.

Previous analysis of frequencies in stepped spillway flows are limited to skimming flows (Guenther et al., 2013) and transition flows (Kramer and Chanson, 2018). Within transition flows on a stepped

(a) Average flow depth in step cavities (VO = visual observation; PS = pressure sensor); Comparison with theoretical prediction for fully ventilated step cavity

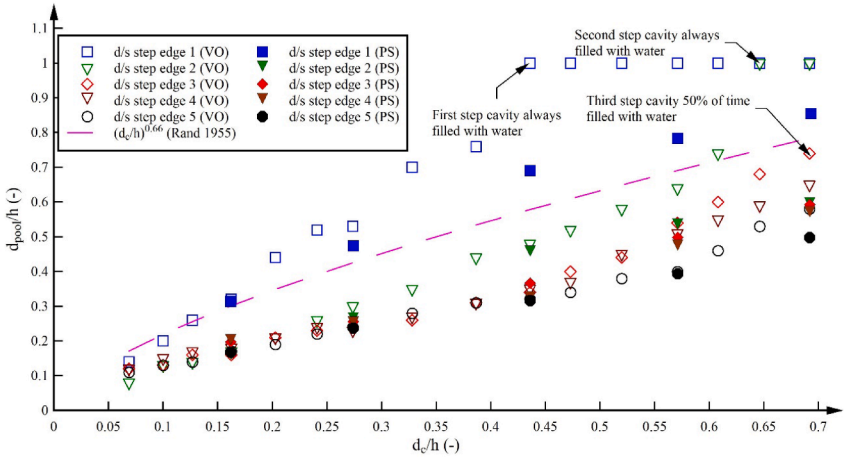

(b) Fluctuations of water levels in step cavities

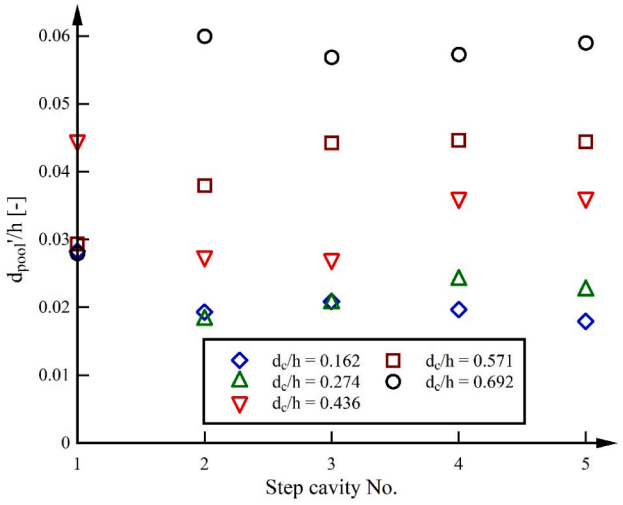

(c) Frequencies of fluctuations in step cavities (Bold symbols = major frequencies; Hollow symbols = secondary frequencies)

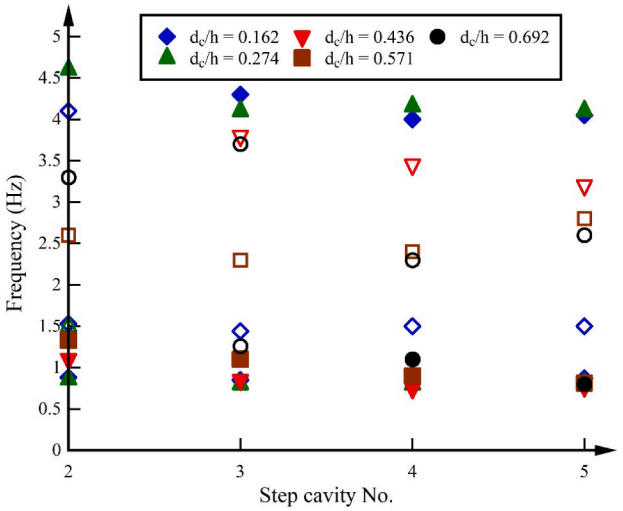

Fig. 7. Development of water depths and characteristic frequencies in step cavities downstream (d/s) of step edges along the stepped chute.

chute with $\theta = 45°$, Kramer and Chanson (2018) observed pool depth frequencies between 1.5 and 3 Hz with an average of 2.7 Hz, based upon a visual technique. Guenther et al. (2013) visually analyzed the cavity ejection frequencies in skimming flows on a stepped spillway with $\theta = 26.6°$ identifying frequencies between 0.33 and 0.66 Hz. The dimensionless frequencies of Guenther et al. (2013) were $0.03 < Freq \times h/V_c < 0.06$ and of Kramer and Chanson (2018) $0.26 < Freq \times h/V_c < 0.38$, while the present data were within a wider range $0.2 < Freq \times h/V_c < 2.4$ (including secondary and multiple dominant frequencies). While the transition flow frequencies were of a similar order of magnitude compared to the present nappe flow observations, there appears to be a distinct difference in characteristic frequencies for the different flow regimes. Further research is needed to identify the effect of channel slope and scale upon the characteristic frequencies.

4. Air-water flow characteristics

Detailed measurements of the air-water flow properties were conducted with the double-tip conductivity probe at step edges and at two locations along the horizontal step face, characterized by air-water flows mostly parallel to the horizontal step face (Fig. 2b, Table 2). At each measurement location, the raw data provided information about a range of air-water flow properties and parameters. Herein, typical distributions of void fraction, bubble count rate, interfacial velocity and interfacial area are presented in Section 4.1, while typical air-water flow parameters along the stepped chute are shown in Section 4.2. The data represented the most detailed documentation of air-water flow properties in nappe flows to date. All distributions of the basic air-water flow properties C, F and V are added as supplementary materials to aid the interpretation of results.

4.1. Distributions of air-water flow properties

4.1.1. Void fraction

Fig. 8 illustrates typical void fraction distributions as a function of the dimensionless vertical elevation above the horizontal step face y/Y_{90}, where Y_{90} is the characteristic flow depth with $C = 0.9$. Fig. 8a shows the evolution of void fraction distributions along the stepped chute for one discharge, highlighting the difference in void fraction profiles at and between step edges as well as the evolution of C along the chute. For the discharge in Fig. 8a, at the upstream end, the void fraction distributions resembled typical S-shape profiles while the profiles further downstream were similar to a jet-like profile. The

(a) Void fraction distributions for $q_w = 0.319$ m²/s, $d_c/h = 0.436$, Re = 1.2×10^6

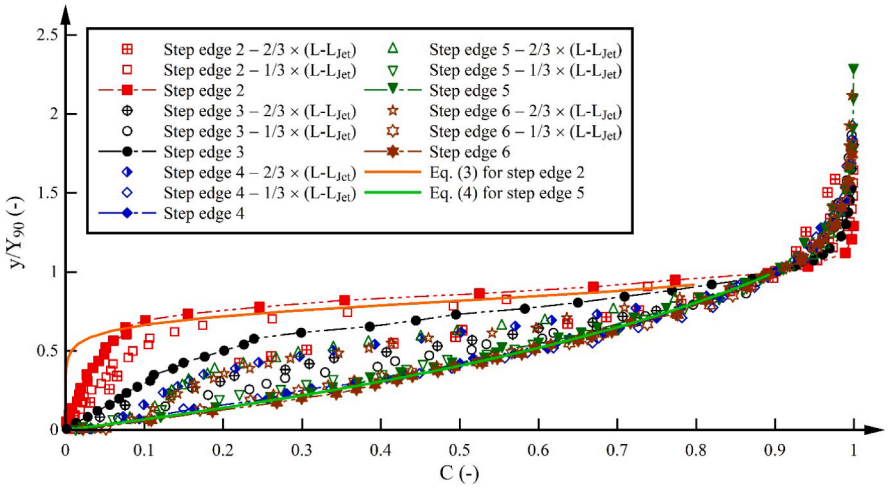

(b) Void fraction distributions at last three step edges for all flow rates

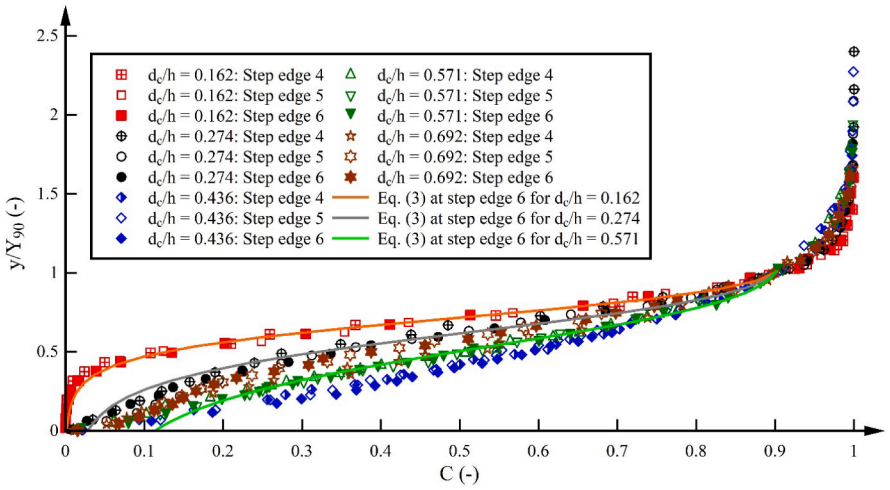

Fig. 8. Dimensionless distributions of void fractions along the stepped spillway in nappe flows; comparison with adjective diffusion Eqs. (3) and (4).

shapes of the void fraction profiles depended upon the discharge and the location downstream of the jet impact. For the lower discharges $d_c/h \leq 0.436$, both S-shape and jet-like void fraction profiles were observed including at step edges for $d_c/h = 0.436$ (Fig. 8a) as well as along the horizontal section downstream of the jet impact ($d_c/h \leq 0.274$). For the largest discharges, all data at and upstream of step edges showed S-shape profiles. Fig. 8b illustrates void fraction profiles for the last three step edges and for all flow configurations, highlighting S-shape profiles for all flow rates apart from $d_c/h = 0.436$. Fig. 8 shows also the close agreement in void fraction distributions at and upstream of consecutive step edges, highlighting the uniformity in void fractions towards the downstream end of the stepped chute independent of the flow rates.

In Fig. 8, the void fraction data were compared with the advective diffusion equation for air-bubbles in skimming flows with S-shape profiles (Chanson and Toombes, 2002b):

$$C = 1 - tanh^2\left(K' - \frac{y/Y_{90}}{2 \times D_o} + \frac{(y/Y_{90} - 1/3)^3}{3 \times D_o}\right) \quad (3)$$

and with the jet-like void fraction profiles which were developed for transition flows (Chanson and Toombes, 2004):

$$C = K'' \times (1 - exp(-\alpha \times y/Y_{90})) \quad (4)$$

In Eqs. (3) and (4), K' is an integration constant and D_o, K'' and α are functions of the mean void fraction in a cross-section C_{mean} only:

$$C_{mean} = K'' - (0.9/\alpha) \quad (5)$$

$$K'' = 0.9/(1 - e^{-\alpha}) \quad (6)$$

Both Eqs. (3) and (4) are added in Fig. 8 for selected data to highlight the close resemblance between advective diffusion equation and void fraction data in nappe flows. Note that the void fraction data deviated from the advective diffusion equation downstream of the first step edge for all discharges (Fig. 8a). The present observations highlighted the complexity of nappe flows including the evolution of void fractions along the stepped chute and the non-uniformity for different flow rates. These observations were consistent with the visual observations of unsteadiness and cavity fluctuations commonly associated with transition flows.

4.1.2. Bubble count rate and interfacial area

Fig. 9a illustrates typical dimensionless bubble count rate distributions $F \times d_c/V_c$ as a function of y/Y_{90} for one discharge. Similar bubble count rate distributions were also observed for all other flow rates in the present study. Downstream of the jet impact of the first jet, the flow became rapidly aerated. Further downstream, the number of air

(a) Bubble count rate distributions for $q_w = 0.159$ m²/s, $d_c/h = 0.274$, Re = 6.3×10^5

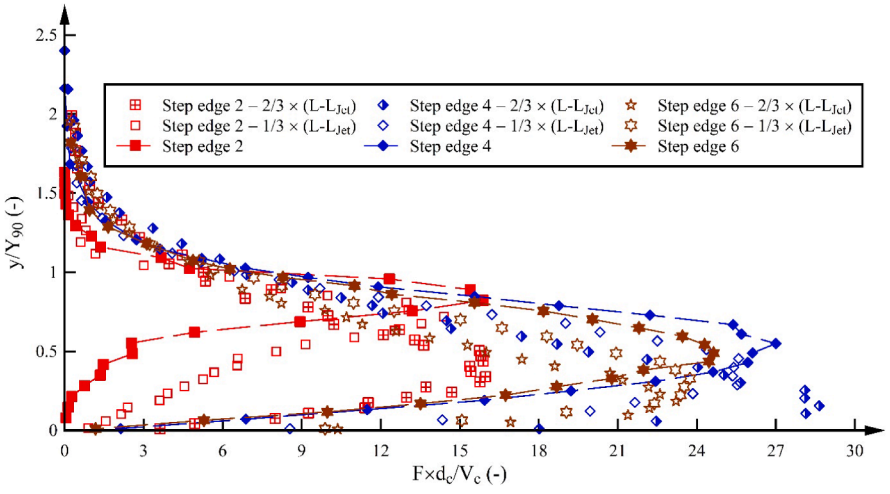

(b) Self-similarity in bubble count rate distributions towards the downstream end of the stepped chute for selected flow rates

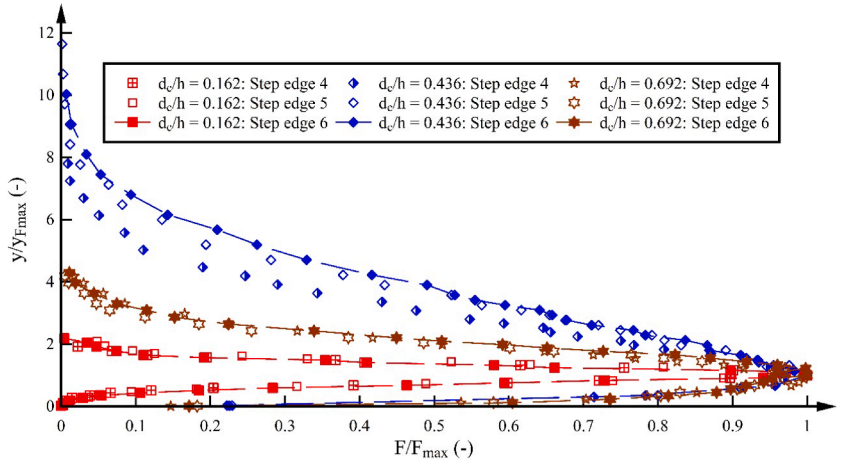

Fig. 9. Dimensionless distributions of bubble count rate and interfacial area along the stepped spillway in nappe flows.

(c) Relationship between void fraction and bubble count rate for all present data; Comparison with parabolic distribution and Equation (7)

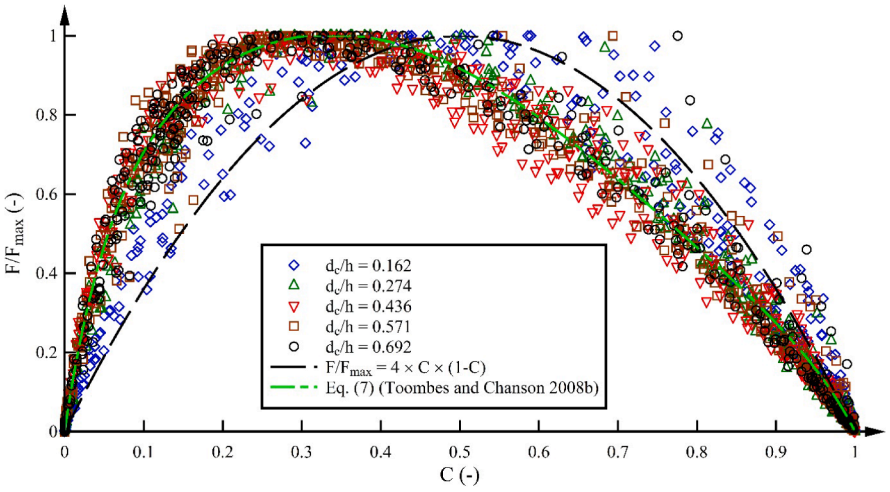

(d) Interfacial area distributions for q_w = 0.637 m²/s, d_c/h = 0.692, Re = 2.5×10⁶

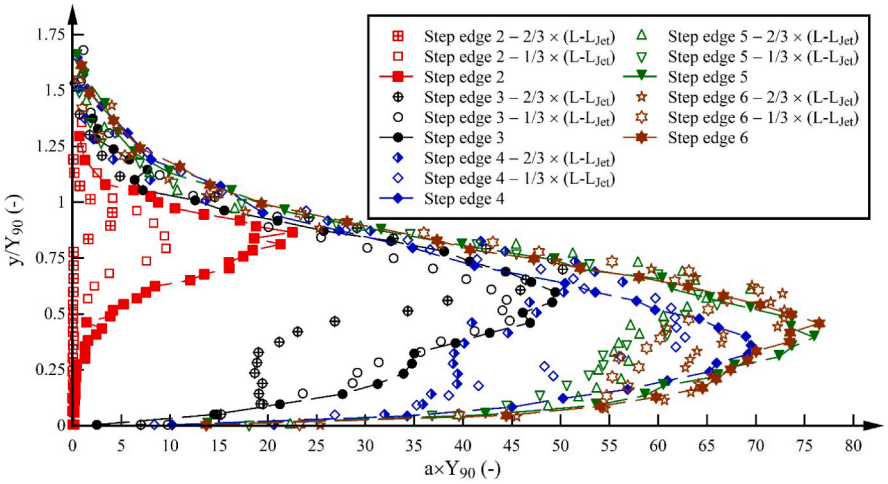

Fig. 9. (*continued*)

bubbles increased approaching equilibrium conditions in the maximum number of bubbles recorded in a cross-section F_{max} as well as in the shapes at and upstream of the step edges. Fig. 9b shows typical dimensionless bubble count rates F/F_{max} as a function of the dimensionless flow depth y/y_{Fmax} where y_{Fmax} is the flow depth corresponding to F_{max}. Towards the downstream end of the stepped chute, the bubble count rate distributions showed self-similarity and uniformity for respective discharges and at consecutive step edges (Fig. 9b). Fig. 9b shows also that there is no self-similarity for different flow rates. The bubble count rate distributions for d_c/h = 0.436 were above the other distributions indicating a stronger flow aeration across the full air-water flow column. This observation was consistent with the void fraction for d_c/h = 0.436 which formed the lowest envelope in void fraction distributions (Fig. 8b).

All data in the present study showed significant numbers of air bubbles, much larger than reported previously in nappe flows (e.g. Toombes and Chanson, 2008b). It is believed that the large scale of the present study limited scale effects which strongly affect bubble count rates and other microscopic air-water flow properties (Felder and Chanson, 2017).

All bubble count rate profiles highlighted typical profiles with very low values of F close to the step face and above the air-water flows as well as maximum values in the bulk of the flows. While the bubble count rate distributions were consistent with previous studies of air-water flows on stepped spillways, it appeared that the maximum bubble count rate values were much closer to the horizontal step face (Fig. 9). Fig. 9c emphasizes this observation in an illustration of void fraction C as a function of dimensionless bubble count rate F/F_{max}. For the lowest discharge d_c/h = 0.162 and for the upstream profiles for all other discharges, the maximum bubble count rate was close to C = 0.5, i.e. within the bulk of the flow typically associated with the strongest air-water flow interactions (Felder and Chanson, 2016a). The data for the lowest discharge compared reasonably well with a parabolic relationship between void fraction and bubble count rate (Fig. 9c). However, at all other locations and for $d_c/h \geq 0.274$, the maximum bubble count rate occurred for much lower void fractions than reported before, i.e. $0.2 < C < 0.4$. It appears that the nappe flow regime in the present study was characterized by strong concentrations of small bubbles next to the horizontal step face. It is believed that this feature is a characteristic feature of nappe flows and linked with the impact of the jet upon the horizontal step face and a jet-like propagation of the air-water flows further downstream. The relationship between C and F/F_{max} was also compared with the modified parabolic model of Toombes and Chanson (2008b) accounting for the different average air bubble and

water droplet chord sizes ch_{air} and ch_{water} and the variation of these chord sizes with the local void fraction:

$$\frac{F}{F_{max}} = \frac{1}{\left(1 + \left(\frac{ch_{water}}{ch_{air}} - 1\right) \times C\right) \times (1 - b \times (1 - 2 \times C)^4)} \times \frac{C \times (1 - C)}{C_{Fmax}^2} \quad (7)$$

where b is a coefficient of maximum variation in chord sizes and C_{Fmax} is the void fraction corresponding to F_{max}. For the data in the present study, on average ch_{water}/ch_{air} = 3.45 and b = 0.4. Eq. (7) is added in Fig. 9c showing a strong agreement with the experimental data. While the magnitude of the coefficient b was comparable to previous studies, the magnitude of ch_{water}/ch_{air} was larger in the present study compared to previously reported results in nappe flows (Toombes and Chanson 2008b) and transition and skimming flows (Felder 2013).

Fig. 9d shows typical dimensionless distributions of the interfacial area a. The interfacial area distributions had similar shapes compared to the bubble count rate data including small values of a next to the step face and above the flow as well as largest values within the bulk of the flow. Fig. 9d shows the distributions for the largest nappe flow discharge in the present study highlighting the close agreement between interfacial area distributions towards the downstream end of the chute. The present observations showed also the large interfacial area values and the reaeration potential of stepped spillways in nappe flows.

4.1.3. Interfacial velocity

The interfacial velocities represent the average travel time of the air-water flow mixture at each measurement location irrespective of the local void fraction. Typical dimensionless interfacial velocity distributions V/V_{90} are shown in Fig. 10 as function of y/Y_{90}, where V_{90} is the characteristic velocity with C = 0.9. Fig. 10a shows typical distributions of V/V_{90} for one discharge at and upstream of step edges while Fig. 10b illustrates velocity data for all discharges at the last three step edges of the chute. All velocity distributions were different from previously reported velocity data on stepped spillways which were closely correlated with a power law. At the measurement location just downstream of the jet impact, the velocity distributions increased almost linearly within a cross-section with the steepest increase for the larger flow rates (Fig. 10a). At the location closer to the step edge, the velocity distributions became more uniform for all discharges. The velocity profiles at the two locations downstream of the jet impact were consistent with the velocity profiles downstream of an overfall presented by Moore (1941).

At the step edges, the distributions depended upon the discharges (Fig. 10b). For the two lowest discharges $d_c/h \leq 0.274$, the velocities remained mostly uniform close to the step face and increased towards the free-surface (Fig. 10b). In contrast, for the largest discharges, the velocity distributions were markedly different with largest velocities close to the step face and an almost linear decrease in velocities with

(a) Interface velocity distributions for q_w = 0.478 m²/s, d_c/h = 0.571, Re = 1.9×10⁶

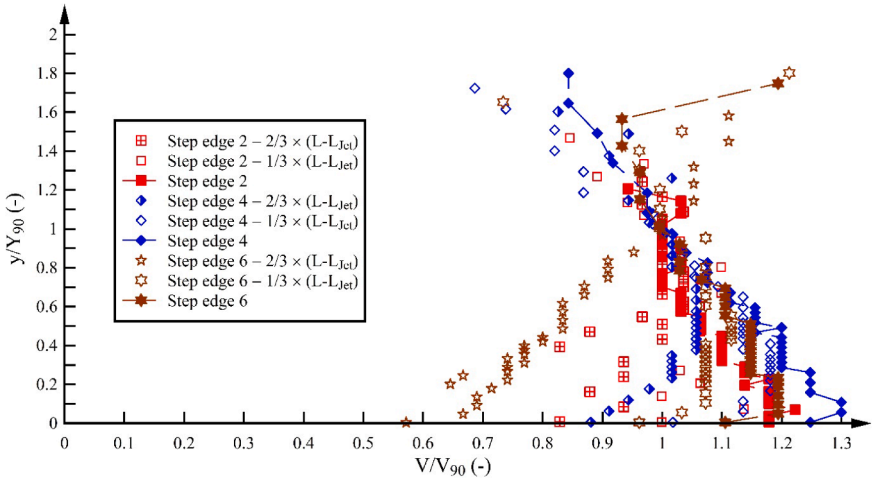

(b) Interface velocity distributions at last three step edges for all flow rates

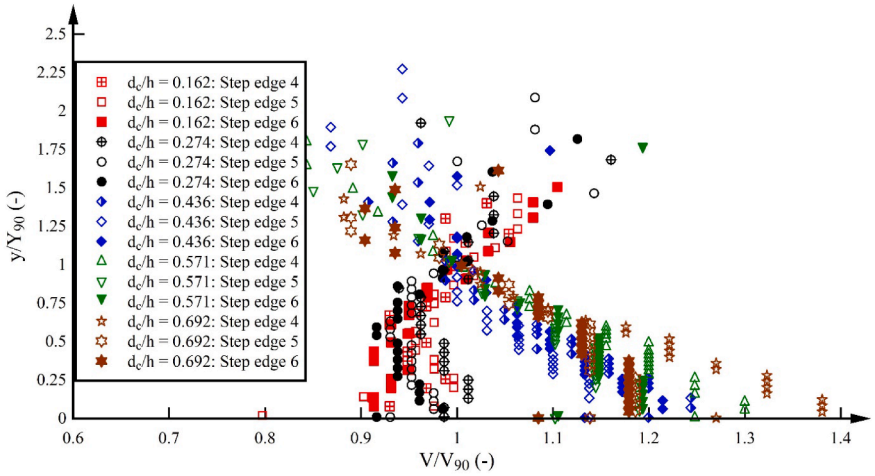

Fig. 10. Dimensionless distributions of interfacial velocity along the stepped spillway in nappe flows.

increasing flow depth. The velocity profiles were consistent with velocity profiles reported of a free overfall (e.g. Hager, 1983) and of a wall jet (e.g. Rajaratnam, 1965) independent of the step edges. In particular for the last two step edges, the velocity profiles were very similar for all discharges suggesting uniform conditions towards the downstream end of the stepped chute (Fig. 10).

4.2. Basic air-water flow parameters along the stepped spillway

In addition to the detailed documentation of the air-water flow properties, several characteristic air-water flow parameters were calculated for all data and at all measurement locations. These characteristic air-water flow parameters are illustrated in Fig. 11 as a function of the dimensionless distance downstream of step edge 1, x/L. The characteristic parameters are the mean void fraction C_{mean} (Fig. 11a), the maximum bubble count rate F_{max} (Fig. 11b), the characteristic flow depth Y_{90} (Fig. 11c) and the characteristic flow velocity V_{90} (Fig. 11d). The uniformity of these parameters at step edges towards the downstream end of the chute are indicated with a dashed line (Fig. 11).

The development of C_{mean} and F_{max} highlighted a steep increase in flow aeration downstream of the first step edge approaching uniform flow conditions of these parameters towards the last two step edges of the chute (Fig. 11a and b). Upstream of the step edges, both parameters showed stronger variation indicating the complexity of the flows including instabilities. Furthermore, the measurement locations varied upstream of the step edges since the jet length was not identical, i.e. L-L_{Jet} differed between step cavities (Fig. 2b and 6). The two lowest discharges were characterized by flow bulking just downstream of the jet impact resulting in an increase in C_{mean} while C_{mean} decreased along the horizontal step face towards step edges linked with buoyancy effects on entrained air bubbles (Fig. 11a). Downstream of the third step edge, little differences at and upstream of step edges were observed for F_{max} with increasing number of bubbles and increasing discharge. A comparison of the five present discharges suggested that the intermediate flow rate of $d_c/h = 0.436$ might be best for optimum flow aeration and air-water mass transfer processes. For this flow rate, C_{mean} was largest at step edges, while F_{max} values were relatively close to the largest two discharges.

The distributions of Y_{90} and V_{90} were consistent with the other two parameters highlighting very uniform parameters for the two lowest discharges and a good agreement at step edges for the largest discharges (Fig. 11c and d). Despite some strong data scatter upstream of the step edges, the present data suggested that the flow may be close to uniform conditions at the downstream end of the chute. Further research is however recommended to test if an increase in sampling duration may be needed to eliminate some of the strong data scatter linked with the flow instabilities towards the downstream end of the flume.

4.3. Discussion

Previous research by Felder and Chanson (2014) found instationary motions on a pooled stepped spillway including jump waves which propagated along the pooled stepped chute. Felder and Chanson (2014) developed a triple decomposition technique to separate the instationarities from the air-water flow signal. The instationary motions

(a) Mean void fraction in a cross-section C_{mean}

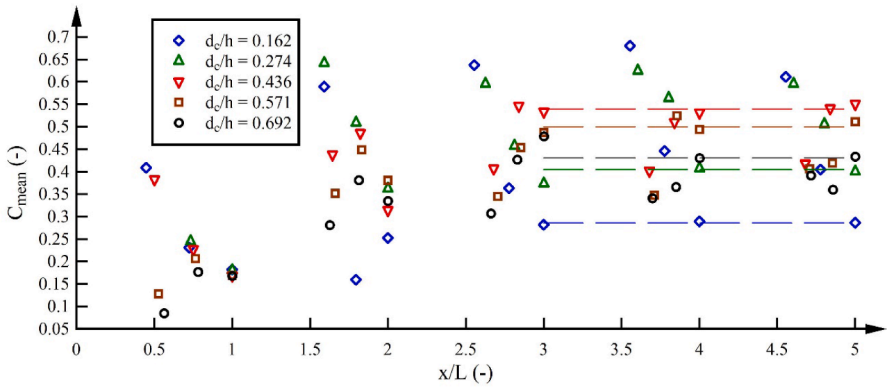

(b) Maximum bubble count rate in a cross-section F_{max}

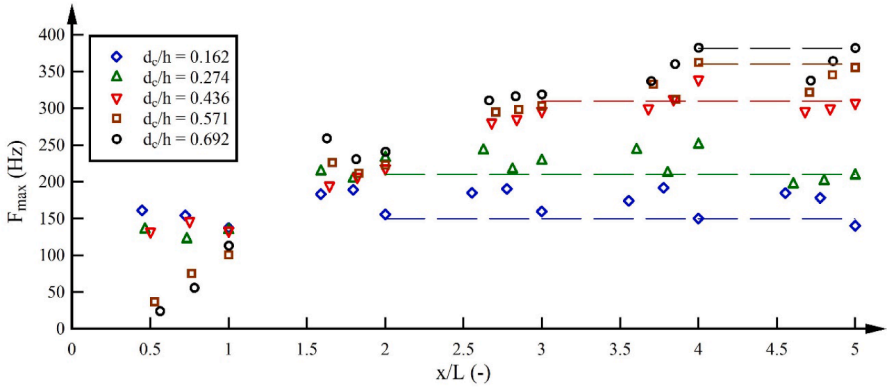

Fig. 11. Characteristic air-water flow parameters along the stepped spillway; dashed lines highlight uniformity of parameters (Note: integer numbers indicate step edges; $x/L = 1$ corresponds to step edge 2).

(c) Characteristic flow depth Y_{90}

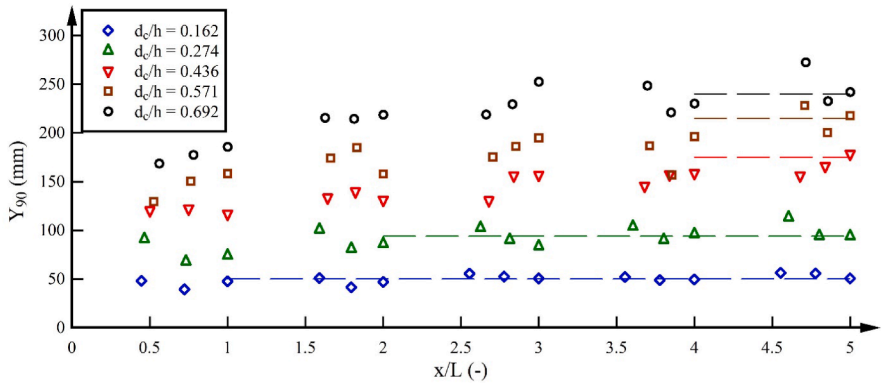

(d) Characteristic flow velocity V_{90}

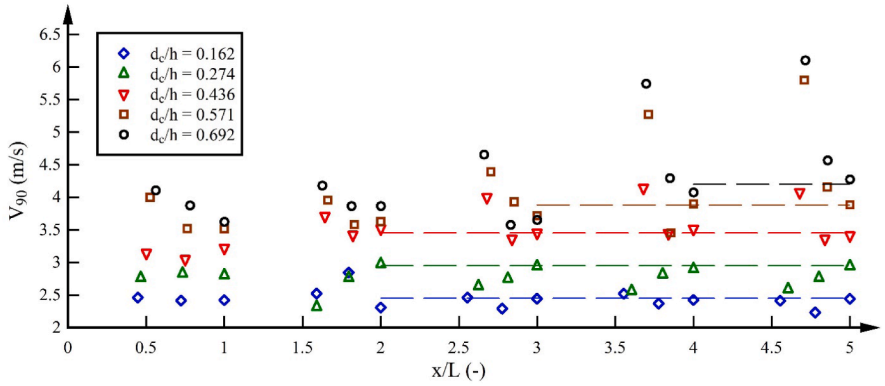

Fig. 11. (*continued*)

in the present study were similar and an application of a triple decomposition technique may be useful for advanced air-water flow properties including turbulence intensities and integral turbulent time and length scales.

Recently Kramer et al. (2019) developed an adaptive window cross-correlation technique which could be applied to the present data set. This method would provide a pseudo-instantaneous velocity time series at each measurement location. These velocity time series could be used for further analysis of the instationary motions in the nappe flow regime including the calculation of turbulence intensities as well as the application of a triple decomposition technique.

5. Energy dissipation performance

The energy dissipation performance at the last step edge was calculated for a range of discharges $0.162 \leq d_c/h \leq 0.692$ based upon the

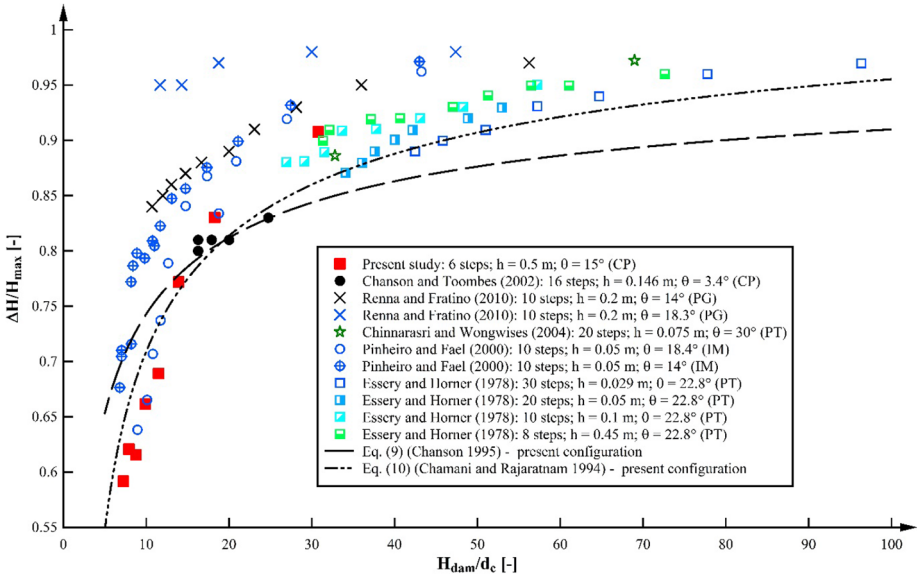

Fig. 12. Energy dissipation rate at the downstream end of the present stepped chute (present H_{dam} = 2.5 m); comparison with other nappe flow data and semi-empirical equations for energy dissipation (Eqs. (9) and (10)); Experimental data based upon CP = conductivity probe; PG = pointer gauge; PT = Pitot tube; IM = Indirect method with hydraulic jump.

conductivity probe measurements. Fig. 12 illustrates the dimensionless energy dissipation rate $\Delta H/H_{max}$ as a function of the dimensionless dam height H_{dam}/d_c, where H_{max} is the maximum head above the broad-crested weir $H_{max} = H_{dam} + 1.5 \times d_c$, H_{dam} is the height of the dam above the last step edge and ΔH is the dissipated energy between the upstream head and the residual head H_{res} at the last step edge, $\Delta H = H_{max} - H_{res}$, with:

$$H_{res} = d + \frac{U_w^2}{2 \times g} = \int_0^{Y_{90}} (1 - C) \times dy + \frac{q_w^2}{2 \times g \times \left(\int_0^{Y_{90}} (1 - C) \times dy\right)^2} \quad (8)$$

The present data were compared with available nappe flow data from previous experimental studies with similarly sloped stepped spillways $3.4 \leq \theta \leq 30°$. Overall, the present data were in good agreement with these previous data revealing a decrease in energy dissipation performance with increasing flow rate. The energy dissipation measurements were based upon different experimental methods and conducted on different experimental facilities which can explain the differences in experimental energy dissipation data (Fig. 12). Fig. 12 shows also a comparison of the present data with two semi-empirical equations including the equation by Chanson (1995) for nappe flows with fully developed hydraulic jumps:

$$\frac{\Delta H}{H_{max}} = 1 - \left(\frac{0.54 \times \left(\frac{d_c}{h}\right)^{0.275} + 1.715 \times \left(\frac{d_c}{h}\right)^{-0.55}}{\frac{H_{dam}}{d_c} + 1.5} \right) \quad (9)$$

and the equation by Chamani and Rajaratnam (1994) which was developed from the data of Horner (1969) for $0.421 \leq h/L \leq 0.842$:

$$\frac{\Delta H}{H_{max}} = 1 - \left(\frac{(1 - \alpha)^N \times \left(\frac{h}{d_c} + 1.5\right) + \frac{h}{d_c} \times \sum_{i=1}^{N-1} (1 - \alpha)^i}{\frac{H_{dam}}{d_c} + 1.5} \right) \quad (10)$$

with

$$\alpha = 0.3 - 0.35 \times \frac{h}{L} - \left(0.54 + 0.27 \times \frac{h}{L}\right) log\frac{d_c}{h} \quad (11)$$

and N the number of steps. Eq. (9) did not match the present data well. Eq. (9) is only valid in nappe flows with hydraulic jumps and therefore not directly applicable to the experimental data in Fig. 12. Eq. (10) did match the present data quite well (Fig. 12) and it has been tested successfully against other experimental nappe flow data. Therefore, the authors recommend using Eq. (10) for any calculation of energy dissipation performances in nappe flows and for $h/L > 0.25$.

6. Reaeration efficiency

Dissolved oxygen measurements were conducted at 0.1 Hz within step cavities 3–6 (Fig. 2) and the aeration efficiency at 20 °C E_{20} was computed as:

$$E_{20} = \frac{C_d - C_u}{C_s - C_u} \quad (12)$$

where C_d is the dissolved oxygen concentration in step cavities 3 to 6, C_u the dissolved oxygen concentration in the header tank and C_s the dissolved oxygen concentration at saturation. The time-averaged data are presented in Fig. 13a as a function of H_{dam}/d_c. The data are shown for different dam heights representing the drop from the upstream end of the stepped chute to the respective step cavity 3–6. For each of the present data series, multiple data points for the same value of H_{dam}/d_c corresponded to the results of independent tests. This enabled appreciating the variability of the results. The present data were compared with dissolved oxygen measurements by Essery et al. (1978), Toombes and Chanson (2005) and Baylar et al. (2007) for similar dam height and for the nappe flow regime. The present data were in agreement with these previous studies despite strong data scatter for all data (Fig. 13a). For $H_{dam} = 2$ m, the present data agreed particularly well with the results of Essery et al. (1978), while the data of Toombes and Chanson (2005) indicated much lower aeration efficiency which may be linked with the mild slope of $\theta = 3.4°$ in their study (Fig. 13a). Overall, the aeration efficiency decreased with increasing discharge for constant dam heights. At constant discharge and step height, the oxygen transfer increased with increasing dam height.

The present data with $h = 0.5$ m and $\theta = 15°$ were well correlated by a simple linear equation to H_{dam} and the specific discharge

$$E_{20} = 0.1993 \times \frac{H_{dam}}{q_w^{0.125}} \quad (13)$$

The close agreement between experimental data of E_{20} and Eq. (13) is shown in Fig. 13b. Selected nappe flow data of Essery et al. (1978) with $h = 0.5$ m are added in Fig. 13b showing also a good agreement. However, other data of Essery et al. (1978) with smaller step heights are not well correlated by Eq. (13) and further large-scale experiments are needed to assess the influences of step height and channel slope upon the aeration efficiency.

Additional dissolved oxygen measurements were conducted at several locations within the non-aerated flow region of the same step cavity to assess potential variations in dissolved oxygen along the step cavity. These results showed little differences in reaeration within the step cavity and only the data at $L_{Jet,min}$ were further considered.

For the air-water flow data, the aeration efficiency was also estimated based upon the conductivity probe measurements following the approach by Toombes and Chanson (2005) and Felder and Chanson (2015b). The resulting aeration efficiencies were significantly smaller compared to the direct dissolved oxygen measurements resulting in

(a) Comparison of present aeration efficiency with previous nappe flow data

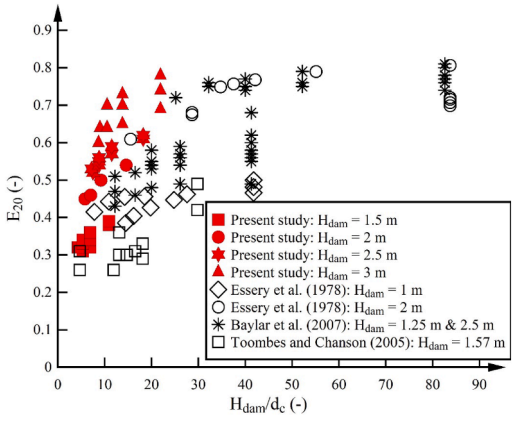

(b) Comparison of measured aeration efficiencies with those predicted from Eq. (13) for $h = 0.5$ m

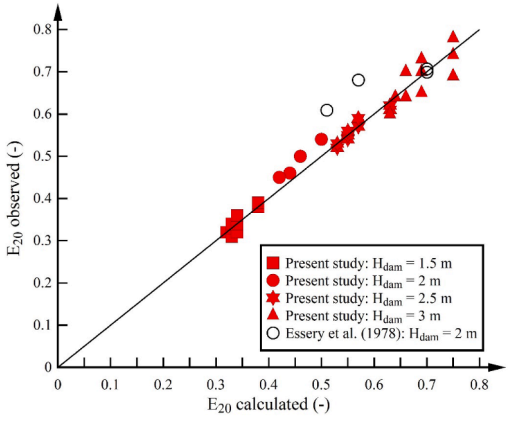

Fig. 13. Aeration efficiency at various steps of the present stepped chute.

estimated values of $12.7 < E_{20} < 21.5$ with decreasing efficiency with increasing discharge. The calculation of the efficiency based upon the air-water flow data had several shortcomings including the start of the calculation just upstream of step 2 which ignored potential reaeration upstream of this location. The air-water flow measurements were limited to cross-sections at the downstream end of the horizontal step faces and the step edges resulting in a very rough averaging of the aeration between successive steps including missing aeration data of the jet itself, the impact region and the additional contributing area underneath the jet. Additional limitations were linked with the probe tip sizes of the conductivity probe, and the calculation approach itself which relied on assumptions of uniform circular bubbles, a constant liquid film coefficient and the missing contribution of the ejected droplets above the flow. Further research is needed to link the air-water flow data and energy dissipation performances with the aeration efficiency in stepped spillways particularly in the nappe flow regime which is characterized by strong variations in air-water flows along the chute.

7. Discussion

Air-water flows at laboratory scale can be affected by scale effects (Kobus, 1984). Previous scale studies of air-water flows on stepped spillways highlighted that particularly microscopic air-water flow properties including bubble count rate and bubble sizes are strongly affected by scale effects (Felder and Chanson, 2017). The steps in the present study had prototype-scale height ($h = 0.5$ m) allowing the most detailed observation of the nappe flow regime to date including the air-water flow features. For example, the bubble count rate in the present study, i.e. the number of air-water interfaces within the flows, were significantly larger compared to previous nappe flow experiments at smaller scale. The present study was conducted for Reynolds number with two orders of magnitude range and up to a maximum of $Re = 2.5 \times 10^6$. Such Reynolds numbers were one order of magnitude larger compared to previous experimental studies of air-water flows in nappe flows. At this large scale, the experiments allowed also a more detailed observation of the nappe flow features compared to previous scale experiments including the development of the nappe flows and the occurrence of instationarities along the stepped chute as well as the uniform flow conditions downstream of the fourth step edge for all flow conditions. Due to the large-scale experiments, the findings may be directly applicable to the design of stepped spillways operating within the nappe flow regime.

To facilitate the dissolved oxygen measurements for prototype-scale step heights, the width of the stepped chute in the present study had to be minimized to $W = 0.2$ m. This channel width is smaller compared to most previous studies (Table 1). The channel width resulted in sidewall effects which may have dampened some of the three-dimensional flow features of nappe flows typically observed in prototype stepped chutes with much larger width (Fig. 1). Little information is known about the effects of channel width upon the air-water flow features in stepped spillway flows, apart from a numerical study which suggested effects of channel width on the three-dimensional flows features in the skimming flow regime (Lopes et al. 2017), while experimental air-water flow data in skimming flows for two different channel width showed little effects of the channel width upon the air-water flow data in channel center line (Felder, 2013; Felder and Chanson, 2015c). To assess potential width effects upon the flow features in the present study, air-water flow experiments were conducted at locations $1/4 \times W$ and $3/4 \times W$ at step edge 6 and along the horizontal step face upstream. A comparative analysis of the air-water flow properties at these quarter locations and the centerline was conducted for all discharges showing close similarity between all air-water flow properties independent of the discharge and the cross-flume location. While the void fraction distributions showed no differences, the flow velocities were slightly larger and the flow depth slightly smaller in channel centerline. These observations indicated small effects of the sidewalls. Visual observations from top view showed little differences in flow patterns across the channel width. Further research at similar large scale is needed to identify potential effects of the channel width upon nappe flows.

8. Conclusions

A unique experimental study was conducted on a stepped spillway model with prototype-scale steps height providing the most detailed characterization of nappe flows to date. The experiments were conducted for a wide range of nappe flow discharges highlighting that nappe flows is mostly associated with supercritical flows without hydraulic jumps, while only for very small flow rates ($d_c/h \leq 0.057$) nappe flows with hydraulic jumps were found. This finding is valid for the present slope of 15 degrees, but also likely applicable for any stepped spillway with steeper slope.

Detailed observations of the flow patterns documented the evolution of nappe flows along the stepped chute including the development of instationarities such as jump waves and fluctuations of the water levels within the step cavities, which were associated with the impingement of the jet upon the horizontal step face. With increasing discharge and increasing distance along the stepped chute the free-surface instabilities increased resulting in droplet ejections of four times the step height. The jet characteristics and the flow depth within the step cavities were documented showing some deviation from theory linked with a non-ventilated first step cavity. A pressure sensor within the step cavity provided the characteristic frequencies of the nappe flows resulting in a range of frequencies between 0.75 and 4.5 Hz with the most dominant frequency of about 1 Hz for all flow rates. Visual observations confirmed the occurrence of jump waves about every second. The visual observations highlighted that the common perception of nappe flows as a regular occurrence of similar nappes is not correct at this large scale confirming prototype observations of some unsteadiness in the nappe flow regime.

Detailed measurements of the air-water flow properties were conducted with a double-tip conductivity probe at all step edges and at locations along the horizontal step face upstream of the step edges. The results highlighted the strong aeration of the flows for all discharges and the evolution of the air-water nappe flows along the chute. While the air-water flow properties were varied at the first few step edges, the flows appeared to be uniform downstream of step edge 4 for all flow rates despite some data scatter associated with the instationarities. The void fraction distributions showed both S-shape and jet-like profiles highlighting the complexity of the flows while the intermediate flow rate of $d_c/h = 0.436$ appeared to be the most aerated flow condition. The bubble count rate and interfacial area followed typical distributions with maximum number of bubbles just above the step face for void fractions between $0.2 < C < 0.4$, i.e. lower compared to previously reported values for stepped spillway flows. It is believed that this is associated with the jet-like flows downstream of the jet impact which was also visible in the jet-like interfacial velocity distributions at and upstream of the step edges. Several characteristic air-water flow parameters confirmed the uniformity of the flows towards the downstream end of the chute.

The energy dissipation rate was recorded at the last step edge showing strong dissipation potential of stepped spillways in nappe flows. A comparison with previous studies showed relatively good agreement with strongest differences with studies not conducted with conductivity probes but with indirect methods to assess the energy dissipation. The data were well correlated by a semi-empirical equation for energy dissipation in nappe flows. At several steps, the dissolved oxygen content was measured highlighting an increase in aeration efficiency with increasing dam height. The present data were overall in agreement with the limited previous studies of aeration efficiency and all present data collapsed into a simple linear prediction of aeration efficiency for stepped chutes with $h = 0.5$ m.

The present study provided important insights into the nappe flow

regime at large scale which should provide spillway designers with confidence of the air-water flow features and patterns in nappe flows. However further research is recommended to document the evolution of the air-water flow features along the stepped chute in more detail including the jet itself and the jet impact, and to assess any effects of channel width upon the nappe flows.

Declaration of Competing Interest

None.

Acknowledgements

The first author thanks Rob Jenkins (WRL, UNSW Sydney) for the manufacturing of the conductivity probe and researchers at HECE, Liege University for collaboration. The last two authors thank the Cebedeau association for providing the dissolved oxygen probes.

Funding

This research did not receive any specific grant from funding agencies in the public, commercial, or not-for-profit sectors.

Appendix A. Supplementary data

Supplementary data to this article can be found online at https://doi.org/10.1016/j.jher.2019.07.004.

References

Baylar, A., Bagatur, T., Emiroglu, M.E., 2007. Prediction of oxygen content of nappe, transition and skimming flow regimes in stepped-channel chutes. J. Environ. Eng. Sci. 6, 201–208. https://doi.org/10.1139/s06-048.

Bayon, A., Toro, J.P., Bombardelli, F.A., Matos, J., López-Jiménez, P.A., 2018. Influence of VOF technique, turbulence model and discretization scheme on the numerical simulation of the non-aerated, skimming flow in stepped spillways. J. Hydro-environ. Res. 19, 137–149. https://doi.org/10.1016/j.jher.2017.10.002.

Bung, D.B., Valero, D., 2016. Optical flow estimation in aerated flows. J. Hydraul. Res. 54 (5), 575–580. https://doi.org/10.1080/00221686.2016.1173600.

Chamani, M.R., Rajaratnam, N., 1994. Jet flow on stepped spillways. J. Hydraul. Eng. 120 (2), 254–259. https://doi.org/10.1061/(ASCE)0733-9429(1994) 120:2(254).

Chanson, H., 1994. Hydraulics of nappe flow regime above stepped chutes and spillways. Aust. Civil Eng. Trans. CE 36 (1), 69–76.

Chanson, H., 1995. Hydraulic Design of Stepped Cascades, Channels. Weirs and Spillways, Pergamon, Oxford, UK.

Chanson, H., Bung, D., Matos, J., 2015. Stepped spillways and cascades. In: Chanson, H. (Ed.), Energy Dissipation in Hydraulic Structures. IAHR Monograph. CRC Press, Taylor & Francis Group, Leiden, The Netherlands, pp. 45–64.

Chanson, H., Toombes, L., 1998. Supercritical flow at an abrupt drop: flow patterns and aeration. Can. J. Civ. Eng. 25 (5), 956–966. https://doi.org/10.1139/l98-013.

Chanson, H., Toombes, L., 2002a. Energy dissipation and air entrainment in a stepped storm waterway: an experimental study. J. Irrig. Drain. Eng. 128 (5), 305–315. https://doi.org/10.1061/(ASCE)0733-9437(2002) 128:5(305).

Chanson, H., Toombes, L., 2002b. Air-water flows down stepped chutes: turbulence and flow structure observations. Int. J. Multiphase Flow. 28 (11), 1737–1761. https://doi.org/10.1016/S0301-9322(02)00089-7.

Chanson, H., Toombes, L., 2004. Hydraulics of stepped chutes: the transition flow. J. Hydraul. Res. 42 (1), 43–54. https://doi.org/10.1080/00221686.2004.9641182.

Chinnarasri, C., Wongwises, S., 2004. Flow regimes and energy loss on chutes with upward inclined steps. Can. J. Civ. Eng. 31 (5), 870–879. https://doi.org/10.1139/l04-052.

Erpicum, S., Lodomez, M., Savatier, J., Archambeau, P., Dewals, B., Pirotton, M., 2016. Physical modeling of an aerating stepped spillway. Proc. 6th IAHR International Symposium on Hydraulic Structures.

Essery, I.T.S., Horner, M.W., 1978. The Hydraulic Design of Stepped Spillways. CIRIA Report No. 33, 2nd Edition, London, UK.

Essery, I.T.S., Tebbutt, T.H.Y., Rasaratnam, S.K., 1978. Design of spillways for reaeration of polluted waters. CIRIA Rep. No. 72, London, UK.

Felder, S., 2013. Air-Water Flow Properties on Stepped Spillways for Embankment Dams: Aeration, Energy Dissipation and Turbulence on Uniform, Non-Uniform and Pooled Stepped Chutes. PhD thesis. The University of Queensland, Australia, pp. 504.

Felder, S., 2018. StefanFelder/Air-water-flow-data-analysis-software-for-double-tip-phase-detection-intrusive-probes (Version v1.0). Zenodo. http://doi.org/10.5281/zenodo.2448251.

Felder, S., Chanson, H., 2011. Air-water flow properties in step cavity down a stepped chute. Int. J. Multiphase Flow 37, 732–745. https://doi.org/10.1016/j.ijmultiphaseflow.2011.02.009.

Felder, S., Chanson, H., 2014. Triple decomposition technique in air-water flows: application to instationary flows on a stepped spillway. Int. J. Multiphase Flow 58, 139–153. https://doi.org/10.1016/j.ijmultiphaseflow.2013.09.006.

Felder, S., Chanson, H., 2015a. Phase-detection probe measurements in high-velocity free-surface flows including a discussion of key sampling parameters. Exp. Therm. Fluid Sci. 61, 66–78. https://doi.org/10.1016/j.expthermflusci.2014.10.009.

Felder, S., Chanson, H., 2015b. Aeration and air–water mass transfer on stepped chutes with embankment dam slopes. Environ. Fluid Mech. 15, 695–710. https://doi.org/10.1007/s10652-014-9376-x.

Felder, S., Chanson, H., 2015c. Closure to aeration, flow instabilities, and residual energy on pooled stepped spillways of embankment dams by Stefan Felder and Hubert Chanson. J. Irrig. Drain. Eng. 141 (2). https://doi.org/10.1061/(ASCE)IR.1943-4774.0000783.

Felder, S., Chanson, H., 2016a. Air–water flow characteristics in high-velocity free-surface flows with 50% void fraction. Int. J. Multiphase Flow 85, 186–195. https://doi.org/10.1016/j.ijmultiphaseflow.2016.06.004.

Felder, S., Chanson, H., 2016b. An Experimental Study of Air-water Flows in Hydraulic Jumps with Channel Bed Roughness, WRL Research Rep. 259. Univ. of New South Wales, Sydney, Australia, pp. 166.

Felder, S., Chanson, H., 2017. Scale effects in microscopic air-water flow properties in high-velocity free-surface flows. Exp. Therm. Fluid Sci. 83, 19–36. https://doi.org/10.1016/j.expthermflusci.2016.12.009.

Felder, S., Hohermuth, B., Boes, R.M., 2019. High-velocity air-water flows downstream of sluice gates including selection of optimum phase-detection probe. Int. J. Multiphase Flow (in 2nd review).

Felder, S., Pfister, M., 2017. Comparative analyses of phase-detective intrusive probes in high-velocity air–water flows. Int. J. Multiphase Flow 90, 88–101. https://doi.org/10.1016/j.ijmultiphaseflow.2016.12.009.

Gonzalez, C.A., Chanson, H., 2008. Turbulence manipulation in embankment stepped chute flows: an experimental study. Eur. J. Mech. B. Fluids 27 (4), 388–408. https://doi.org/10.1016/j.euromechflu.2007.09.003.

Guenther, P., Felder, S., Chanson, H., 2013. Flow aeration, cavity processes and energy dissipation on flat and pooled stepped spillways for embankments. Environ. Fluid Mech. 13 (5), 503–525. https://doi.org/10.1007/s10652-013-9277-4.

Hager, W.H., 1983. Hydraulics of plane free overfall. J. Hydraul. Eng. 109 (12), 1683–1697. https://doi.org/10.1061/(ASCE)0733-9429(1983) 109:12(1683).

Hong, Y., Huang, S., Wan, S., 2010. Drop characteristics of free-falling nappe for aerated straight-drop spillway. J. Hydraul. Res. 48 (1), 125–129. https://doi.org/10.1080/00221680903568683.

Horner, M.W., 1969. An Analysis of Flow on Cascades of Steps. Ph.D. Thesis. University of Birmingham, UK, pp. 357.

Kobus, H., 1984. Local Air Entrainment and Detrainment. Proc. Symp on Scale Effects in Modelling Hydraulic Structures. IAHR, Esslingen, Germany.

Kramer, M., Chanson, H., 2018. Transition flow regime on stepped spillways: air–water flow characteristics and step-cavity fluctuations. Environ. Fluid Mech. 18 (4), 947–965. https://doi.org/10.1007/s10652-018-9575-y.

Kramer, M., Valero, D., Chanson, H., Bung, D., 2019. Towards reliable turbulence estimations with phase-detection probes: an adaptive window cross-correlation technique. Exp. Fluids 60 (2). https://doi.org/10.1007/s00348-018-2650-9.

Lopes, P., Leandro, J., Carvalho, R.F., Bung, D.B., 2017. Alternating skimming flow over a stepped spillway. Environ. Fluid Mech. 17 (2), 303–322. https://doi.org/10.1007/s10652-016-9484-x.

Meireles, I., Matos, J., 2009. Skimming flow in the nonaerated region of stepped spillways over embankment dams. J. Hydraul. Eng. 135 (8), 685–689. https://doi.org/10.1061/(ASCE)HY.1943-7900.0000047.

Moore, W.L., 1941. Energy loss at the base of a free overfall. Trans. ASCE 108, 1343–1360.

Ohtsu, I., Yasuda, Y., 1997. Characteristics of flow conditions on stepped channels. In: Proc. of the 27th IAHR Biennal Congress. Theme D, San Francisco, 583–588.

Ohtsu, I., Yasuda, Y., Takahashi, M., 2004. Flow characteristics of skimming flows in stepped channels. J. Hydraul. Eng. 130 (9), 860–869. https://doi.org/10.1061/(ASCE)0733-9429(2004) 130:9(860).

Peyras, L., Royet, P., Degoutte, G., 1992. Flow and energy dissipation over stepped gabion weirs. J. Hydraul. Eng. 118 (5), 707–717. https://doi.org/10.1061/(ASCE)0733-9429(1992) 118:5(707).

Pinheiro, A.N., Fael, C.S., 2000. Nappe Flow in Stepped Channels – Occurrence and Energy Dissipation. International Workshop on Hydraulics of Stepped Spillways, Balkema, Zurich, Switzerland, pp. 119–126.

Rajaratnam, N., 1965. The hydraulic jump as a wall jet. J. Hydraulic Divis. 91 (HY5), 107–132.

Rajaratnam, N., 1990. Skimming flow in stepped spillways. J. Hydraul. Eng. 116 (4), 587–591. https://doi.org/10.1061/(ASCE)0733-9429(1990) 116:4(587).

Rand, W., 1955. Flow geometry at straight drop spillways. Proc. ASCE 81 (791), 1–13.

Renna, F.M., Fratino, U., 2010. Nappe flow over horizontal stepped chutes. J. Hydraul. Res. 48 (5), 583–590. https://doi.org/10.1080/00221686.2010.507016.

Sanchez-Juny, M., Pomares, J., Dolz, J., 2000. Pressure Field in Skimming Flor Over a Stepped Spillway. International Workshop on Hydraulics of Stepped Spillways, Balkema, Zurich, Switzerland, 137–145.

Sorensen, R.M., 1985. Stepped spillway hydraulic model investigation. J. Hydraul. Eng. 111 (12), 1461–1472. https://doi.org/10.1061/(ASCE)0733-9429(1985) 111:12(1461).

Stephenson, D., 1979. Gabion Energy Dissipators. In: Proc. 13th ICOLD Congress, New Delhi, India, 50(3), 33–43.

Stephenson, D., 1991. Energy dissipation down stepped spillways. Water Power Dam. Constr. 27–30.

Takahashi, M., Yasuda, Y., Ohtsu, I., 2007. Characteristics of aerated flows in skimming, transition and nappe flows. In: Proc. 32nd IAHR Congress Venice, C2-B (CD-Rom).
Toombes, L., Chanson, H., 2005. Air-water mass transfer on a stepped waterway. J. Environ. Eng. 131 (10), 1377–1386. https://doi.org/10.1061/(ASCE)0733-9372(2005) 131:10(1377).
Toombes, L., Chanson, H., 2008a. Flow patterns in nappe flow regime down low gradient stepped chutes. J. Hydraul. Res. 46 (1), 4–14. https://doi.org/10.1080/00221686.2008.9521838.
Toombes, L., Chanson, H., 2008b. Interfacial aeration and bubble count rate distributions in a supercritical flow past a backward-facing step. Int. J. Multiphase Flow 34 (5), 427–436. https://doi.org/10.1016/j.ijmultiphaseflow.2008.01.005.
Zhang, G., Chanson, H., 2018. Air-water flow properties in stepped chutes with modified step and cavity geometries. Int. J. Multiphase Flow 99, 423–436. https://doi.org/10.1016/j.ijmultiphaseflow.2017.11.009.